Hot-Core Characterization of a Cryogenic D_2 Target at Peak Neutron Production in a Direct-Drive Spherical Implosion

In inertial confinement fusion[1] (ICF), a spherical shell is irradiated either directly by a large number of overlapping laser beams (direct drive) or by x rays produced in a high-Z "hohlraum" (indirect drive).[2] During the laser-driven acceleration phase of an implosion, the target compresses while it converges to the center, then decelerates to peak compression as the core of the target is heated to high temperatures, causing a thermonuclear burn within its fuel. The current goal of ICF research is to achieve ignition and a positive gain, where the amount of energy released through thermonuclear fusion is equal to or higher than the amount of laser energy used to drive the target. The combination of high temperature and areal density (ρR) in the compressed fuel is necessary to ignite the target.[2] This goal is expected to be achieved on the National Ignition Facility (NIF),[2] currently under construction at Lawrence Livermore National Laboratory. In the direct-drive ignition target design[3] for the NIF, a 3.4-mm-diam, 350-μm-thick cryogenic deuterium–tritium (DT) shell is imploded by 192 overlapped laser beams with a total energy of 1.5 MJ. The fusion energy will be released through the nuclear reaction $D + T \rightarrow {}^4He$ (3.5 MeV) + n(14.1 MeV). An expected neutron yield of 2.5×10^{19} (corresponding to a gain of ~45) will be achieved at a fuel temperature of ~30 keV and an areal density of ~1200 mg/cm^2 at peak compression.

While cryogenic DT targets[4,5] will be used for fusion energy production, the current implosion program on the 60-beam, 351-nm OMEGA laser system[6] uses cryogenic D_2 targets to study the relevant implosion physics. The D_2 targets are hydrodynamically equivalent to DT targets, but much simpler to produce and more useful for diagnosing target conditions near peak compression. The primary fusion reaction in D_2 fuel has two branches: (a) $D + D \rightarrow {}^3He$ (0.82 MeV) + n(2.45 MeV), and (b) $D + D \rightarrow T$(1.01 MeV) + p(3.02 MeV). The primary reaction product T reacts with D through the secondary reaction D + T(0 to 1.01 MeV)$\rightarrow {}^4He$ + n(11.9 to 17.2 MeV). Experiments with plastic targets estimated target compression by using the size of the core emission and the ratio of secondary DT to primary DD neutron yields. This technique was first used by Azechi *et al.*[7] and by Cable and Hatchett.[8] In their calculations, the core ρR was inferred from the ratios of secondary to primary yields, assuming the core had uniform temperature and density. For ICF to succeed, it is necessary to infer core temperature–density profiles and directly compare them with hydrocode simulations. Because the target ignition designs are based on hydrocode predictions, they should be benchmarked by the most-comprehensive set of measurements.

Recently Radha *et al.* modeled[9] core temperature–density profiles at peak neutron production in plastic-shell targets. About ten different experimental observations with several different types of targets (having various dopants in a gas fuel and plastic shell) were necessary for a comprehensive characterization of the core conditions.[9] Kurebayashi *et al.*[10] studied the usefulness of secondary particles (neutrons and protons) for hot-core modeling of plastic and cryogenic capsules. The cryogenic D_2 targets cannot have dopants, but because they are much simpler (there is no complication of mixing of different materials in the core), it is possible to characterize them (with the same level of detail as plastic shells) with fewer experimental observables. This article describes experiments where measured primary DD and secondary DT neutron yields, neutron-averaged ion temperatures, and x-ray images at peak neutron production are used to infer the electron-pressure and temperature–density profiles in cryogenic D_2 implosions for the first time. The areal densities of neutron production and "triton-stopping" regions are introduced here to characterize target compression. These quantities are the compression measurements that are extended from the ρR inferred from the ratios of secondary to primary yields. Because they are derived from the temperature–density profiles consistent with experimental measurements, they provide more-accurate measurements of compression.

The experiments were direct-drive implosions of ~920-μm-initial-diam targets with shells that consisted of ~100-μm-thick inner D_2-ice layers and outer 5-μm-thick plastic CD layers.[11] The targets were imploded with a 1-ns square pulse shape with a total on-target energy of ~23 kJ on OMEGA.[6]

The laser beams were smoothed with distributed phase plates,[12] 1-THz two-dimensional smoothing by spectral dispersion,[13] and polarization smoothing[14] using birefringent wedges. The measured experimental yield ratios relative to the predicted yields using 1-D simulations were typically ~30% in a large number of similar implosions. In one implosion, the experimental yield was closer to the predicted yield (59%); therefore, this implosion was used for the analysis presented here. The measured primary DD and secondary DT neutron yields for this implosion were $Y_1 = 1.24 \times 10^{11} \pm 8 \times 10^8$ and $Y_2 = 1.17 \times 10^9 \pm 3 \times 10^7$, respectively.[10] The measured neutron-averaged ion temperature was $T_i = 3.6 \pm 0.5$ keV and the neutron burn width was $\tau = 170 \pm 25$ ps.[11] The core images[11] were measured with an x-ray framing camera with a spatial resolution of ~10 μm, a temporal resolution of ~40 ps, and a 200-μm-thick beryllium filter (which transmitted x rays with energies of more than ~2 keV).

The target core at peak neutron production was characterized by choosing temperature [$T(\mathbf{r})$] and density [$n(\mathbf{r})$] profiles that produced the same primary and secondary neutron yields, the neutron-averaged ion temperature, and the size of x-ray images as measured within experimental uncertainties.[9] In the first stage of modeling, only those temperature–density profiles that were consistent with the primary DD neutron yield and neutron-averaged ion temperature were selected from all possible combinations at a particular electron pressure (the hot core was assumed to be isobaric). In the second stage, profiles consistent with the secondary DT neutron yield were chosen from those selected in the first stage. Similarly, the temperature–density profiles consistent with all neutron measurements were chosen at each electron pressure in the range of 1 to 10 Gbar. Finally, only those temperature–density profiles that were consistent with the size of the x-ray core images were chosen to characterize the hot core at peak neutron production. The following assumptions were used in the core modeling: (1) the core plasma was a fully ionized ideal gas; (2) the core was isobaric $\left[P_e(\mathbf{r}) = \text{const}\right]$ at stagnation; (3) the temperature–density profiles were spherically symmetric; (4) the electron and ion temperatures as well as the densities were equal;[9] (5) the core was static during the time of neutron production τ (therefore, the inferred pressure and temperature–density profiles were considered to be neutron averaged); and (6) the temperature decreased monotonically from the center. These secondary DT neutron yields used Li and Petrasso's plasma stopping powers[15] to calculate the triton's energy loss as it propagated through a 3-D core. The x-ray images were constructed using radiation-transport calculations in a fully ionized deuterium plasma with free-free emission and absorption.[16]

Figure 97.10(a) shows one of the grids used to construct temperature profiles. The temperature step was 250 eV, and the distance step was 20 μm (distance steps of 15, 10, and 5 μm were used in additional, more-detailed grids). The curves show examples of two (out of nearly ~10^{10}) temperature profiles $T(\mathbf{r})$ used in the modeling. The corresponding density profiles $n(\mathbf{r})$ were calculated using $P_e(\mathbf{r}) = n(\mathbf{r}) \times T(\mathbf{r})$. The range of temperatures that satisfy the measured DD neutron yield and neutron-averaged ion temperature (calculated in the first stage of modeling) is shown by the lightly shaded region in Fig. 97.10(b) at an electron pressure of 2.6 Gbar. The results of the second stage of modeling—the temperature profiles consistent with secondary DT neutron yield (in addition to primary DD yield and neutron-averaged ion temperature)—are shown by the darkly shaded region. Similar calculations were conducted for electron pressures in the range from 1 to 10 Gbar. As an example, the ranges of temperature profiles consistent with all neutron measurements for three different electron pressures (1.3, 2.6, and 5.2 Gbar) are shown in Fig. 97.11(a). It was found that for any electron pressure above 1.3 Gbar, temperature–density profiles consistent with all neutron measurements exist; therefore, neutron measurements by themselves are not sufficient to accurately characterize the target core at peak neutron production. The profiles at different pressures, however, would make different sizes of x-ray emission, as can be seen from the profiles shown in Fig. 97.11(b). Therefore, for various temperature–density profiles, the x-ray images were constructed and compared with the one measured at peak neutron production. In these calculations, the transmis-

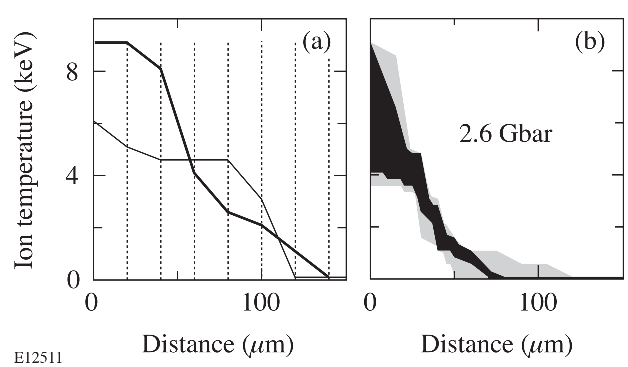

Figure 97.10
(a) The temperature–radius grid. The temperature step is 250 eV, and the distance step is 20 μm, as shown by the vertical dotted lines. The thick and thin solid lines show examples of monotonically decreasing temperature profiles as a function of distance used in core modeling. (b) The range of ion-temperature profiles consistent with the measured primary DD yield and neutron-averaged ion temperature (lightly shaded area), and in addition, the secondary DT yield (darkly shaded area), at electron pressure of 2.6 Gbar.

sion of the Be filter and the x-ray spectral response of the framing camera's gold photocathode were taken into account. The size of the x-ray image is very sensitive to the core pressure [see Fig. 97.11(b)]. The measured core image at peak neutron production is shown in Fig. 97.12(a). Figure 97.12(a) also shows two central lineouts of the measured image in horizontal and vertical directions by thick and thin solid lines. The image is slightly elliptical with FWHM's (full width at half maximum) ranging from about 94 to 100 μm in two perpendicular directions. The measured image is consistent with calculated images in the electron-pressure range from 2.3 to 3.1 Gbar. The shaded area in Fig. 97.12(a) is between the 2.3- and 3.1-Gbar lineouts, and the measured lineouts lie within this area. The ranges of inferred core temperature and density profiles, corresponding to this range of electron pressures, are shown in Figs. 97.12(b) and 97.12(c), respectively. As a result, only a relatively narrow range of temperature–density profiles is consistent with all neutron and x-ray measurements, simultaneously. The dashed curves correspond to simulations using the 1-D hydrocode *LILAC*,[11] which are discussed below.

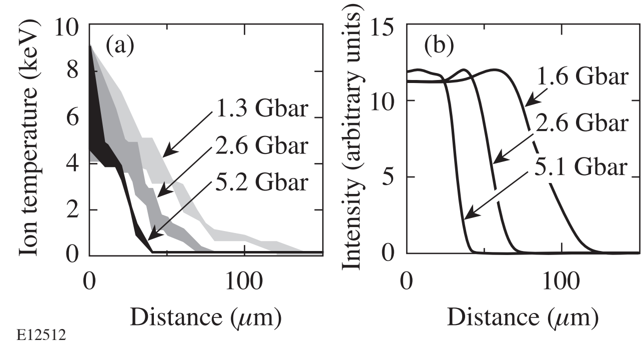

Figure 97.11
(a) The range of temperature profiles that satisfy measured primary DD, secondary DT yields, and neutron-averaged ion temperature, calculated for electron pressures of 1.6 (light), 2.6 (medium), and 5.1 Gbar (darkly shaded area). (b) Examples of x-ray radial lineouts (normalized to their highest values) calculated for the same pressures of 1.6, 2.6, and 5.1 Gbar.

Even though temperature–density profiles contain all information about the core condition, the core ρR has always been a simple and useful measurement[7,8] of target performance in ICF. Modeling based on flat temperature–density profiles[7,8] allows only approximate estimates of the areal density. Detailed temperature–density profiles consistent with all neutron and x-ray measurements are required for accurate determination of the core ρR. The solid line in Fig. 97.13(a) shows a cumulative DD neutron yield as a function of the core areal density, calculated using temperature–density profiles at an electron pressure of 2.6 Gbar. The ρR of the "burn" region of ~10 mg/cm^2 was defined at 95% of the maximum value of the cumulative yield. The burn region ρR inferred from the temperature–density profiles at 1.3 Gbar [see Fig. 97.11(a)] is a factor of 2 smaller. Even though the 1.3-Gbar profiles are consistent with all neutron measurements, they were rejected because they did not predict the measured x-ray images. This means that the core ρR inferred solely from the yield ratio of primary to secondary neutrons (especially using flat profiles that are not consistent with all measurements) could be very

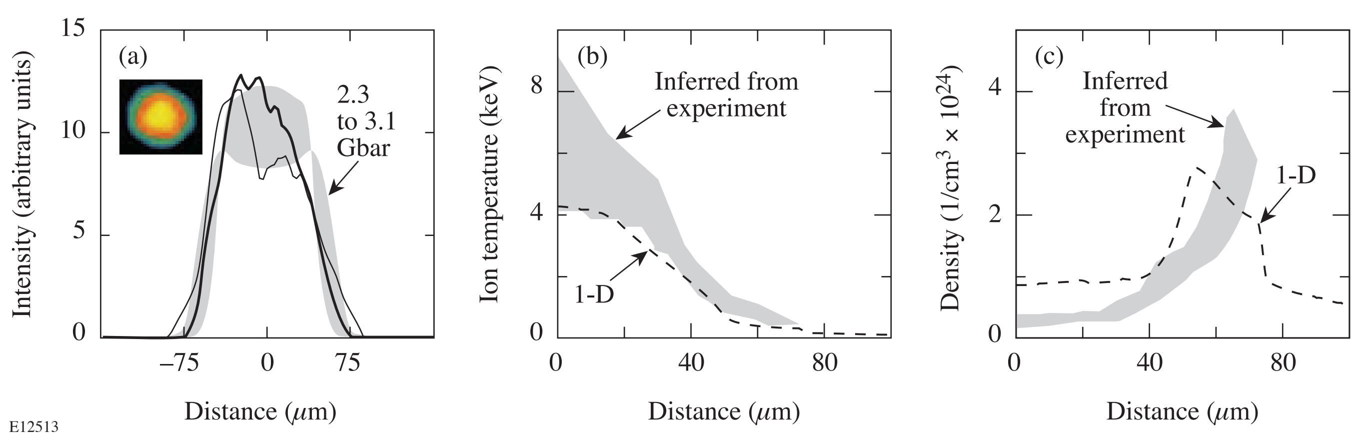

Figure 97.12
(a) X-ray framing camera image of the core at peak neutron production (upper left side); the horizontal and vertical lineouts of this image (thick and thin lines). The shaded area lies in between the lineouts of calculated images at electron pressures of 2.3 and 3.1 Gbar. All lineouts are normalized to the integrated intensities under the curves. The range of (b) core temperature and (c) density profiles corresponding to electron pressures in the range from 2.3 to 3.1 Gbar, which produce sizes of x-ray emission consistent with that of the measured x-ray image (shown by gray areas). The 1-D *LILAC* predictions are shown by dashed lines.

inaccurate. The total target ρR was measured to be ~61 mg/cm^2 at peak neutron production using a downshift in the secondary proton spectra.[10]

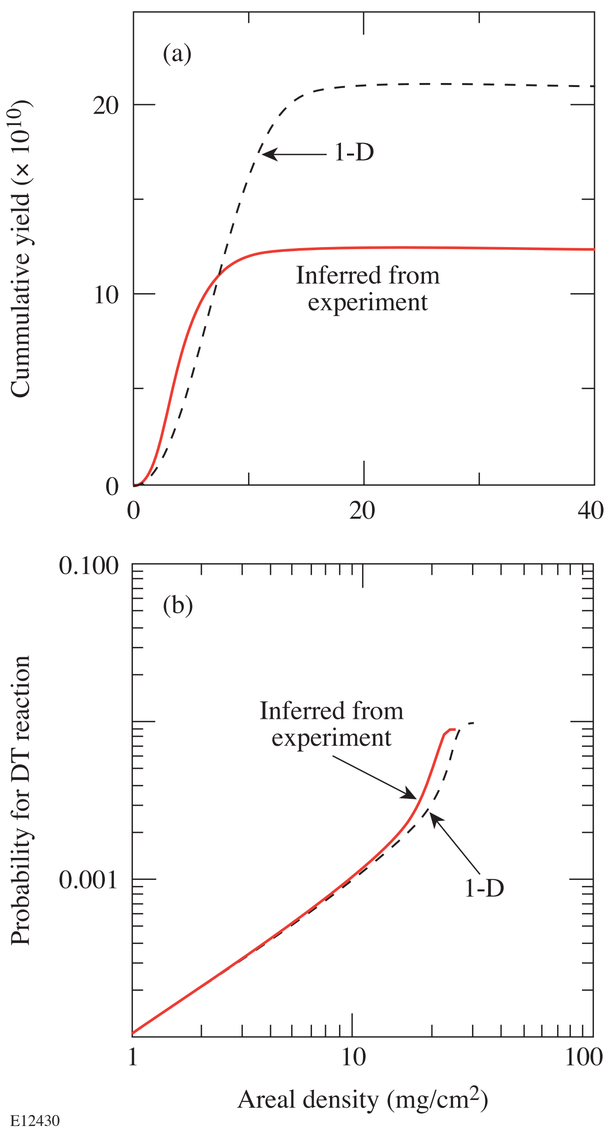

Figure 97.13
(a) Cumulative yields as a function of core ρR, inferred from the experiment, for an electron pressure of 2.6 Gbar (solid curve), and from a 1-D simulation (dashed curve). The ρR's of the "burn" regions (~10 and ~15 mg/cm^2, respectively) were defined at 95% of the maximum value of the cumulative yield. (b) Probability for a secondary DT reaction (equal to a ratio of DT to DD yields) as a function of core ρR, calculated for an electron pressure of 2.6 Gbar (solid curve). The triton probes a core ρR of ~23 mg/cm^2 before being stopped in the core. The dashed curve corresponds to a 1-D simulation with a "triton-stopping" ρR of ~27 mg/cm^2.

The ρR of a "triton-stopping" region is another useful parameter describing the extent of the hot core that is probed by the neutron measurements. The tritons are born in the neutron-production region through the DD fusion reaction. They are slowed down while they move through the core[15] until they are stopped in the target. The triton-slowing rate depends strongly on plasma temperature and density: it is higher in colder, less-dense plasmas;[7,8] therefore the ρR of a triton-stopping region (or the ρR necessary to stop the triton) is higher in hotter, denser cores. As the triton propagates in the core, it can react with deuterium through a secondary DT reaction, producing a secondary DT neutron.[7,8] Figure 97.13(b) shows (by a solid line) the probability for the DT reaction as a function of the core areal density, calculated for the same conditions as in Fig. 97.13(a) at an electron pressure of 2.6 Gbar. In this calculation, the triton is born at the core center and propagates toward the outer surface until it is stopped after probing ~23 mg/cm^2 of the core plasma. The probability for the DT reaction dramatically increases right before the triton is stopped because the DT-reaction cross section increases as the triton slows down in the plasma. Therefore, the secondary DT neutron yield is very sensitive to the temperature–density conditions in the outer part of the hot core, while the primary DD yield is more sensitive to conditions in the central part of the core.

The modeling results were compared with the predictions[11] of a 1-D *LILAC* simulation (dashed lines in Figs. 97.12 and 97.13). The predicted DD neutron yield of 2.1×10^{11} was close to the measured yield of 1.24×10^{11}, while the simulated neutron-averaged ion temperature of 3.1 keV was a little lower than that measured 3.6 keV. As a result, the simulated temperature profile [see Fig. 97.12(b)] was a little lower than the temperature range inferred from the experiment, while the density profile was a little higher [see Fig. 97.12(c)]. In the 1-D simulation, the burn and triton-stopping region ρR's were very close to those inferred from the experiment. In the simulation, the burn ρR was ~15 mg/cm^2 (~10 mg/cm^2 in the experiment) and the triton-stopping region ρR was ~27 mg/cm^2 (~23 mg/cm^2 in the experiment), as shown in Fig. 97.13. Measurements based on monochromatic differential imaging[17,18] of core x rays are planned to infer the time-resolved evolution of D_2-core profiles in the near future, using techniques similar to those described elsewhere.[19]

In conclusion, the compressed-core, electron temperature–density profiles of a cryogenic deuterium (D_2) target have been characterized using measured primary DD and secondary DT yields, neutron-averaged ion temperature, and core x-ray images at peak neutron production. The inferred temperature–density profiles are in good agreement with predictions of the 1-D hydrocode *LILAC*. The electron pressure, burn, and triton-stopping region ρR's were inferred to be 2.7±0.4 Gbar, ~10 mg/cm^2, and ~23 mg/cm^2, respectively.

ACKNOWLEDGMENT

One of the authors (V.A.S.) would like to thank D. C. Wilson for helpful discussions. This work was supported by the U.S. Department of Energy Office of Inertial Confinement Fusion under Cooperative Agreement No. DE-FC03-92SF19460, the University of Rochester, and the New York State Energy Research and Development Authority. The support of DOE does not constitute an endorsement by DOE of the views expressed in this article.

REFERENCES

1. J. Nuckolls *et al*., Nature **239**, 139 (1972).
2. J. D. Lindl, Phys. Plasmas **2**, 3933 (1995).
3. P. W. McKenty, V. N. Goncharov, R. P. J. Town, S. Skupsky, R. Betti, and R. L. McCrory, Phys. Plasmas **8**, 2315 (2001).
4. R. L. McCrory, J. M. Soures, C. P. Verdon, F. J. Marshall, S. A. Letzring, S. Skupsky, T. J. Kessler, R. L. Kremens, J. P. Knauer, H. Kim, J. Delettrez, R. L. Keck, and D. K. Bradley, Nature **335**, 225 (1988).
5. Y. Kitagawa *et al*., Phys. Rev. Lett. **75**, 3130 (1995).
6. T. R. Boehly, D. L. Brown, R. S. Craxton, R. L. Keck, J. P. Knauer, J. H. Kelly, T. J. Kessler, S. A. Kumpan, S. J. Loucks, S. A. Letzring, F. J. Marshall, R. L. McCrory, S. F. B. Morse, W. Seka, J. M. Soures, and C. P. Verdon, Opt. Commun. **133**, 495 (1997).
7. H. Azechi *et al*., Appl. Phys. Lett. **49**, 555 (1986).
8. M. D. Cable and S. P. Hatchett, J. Appl. Phys. **62**, 2233 (1987).
9. P. B. Radha, J. Delettrez, R. Epstein, V. Yu. Glebov, R. Keck, R. L. McCrory, P. McKenty, D. D. Meyerhofer, F. Marshall, S. P. Regan, S. Roberts, T. C. Sangster, W. Seka, S. Skupsky, V. Smalyuk, C. Sorce, C. Stoeckl, J. Soures, R. P. J. Town, B. Yaakobi, J. Frenje, C. K. Li, R. Petrasso, F. Séguin, K. Fletcher, S. Padalino, C. Freeman, N. Izumi, R. Lerche, and T. W. Phillips, Phys. Plasmas **9**, 2208 (2002).
10. S. Kurebayashi, J. A. Frenje, F. H. Séguin, J. R. Rygg, C. K. Li, R. D. Petrasso, V. Yu. Glebov, J. A. Delettrez, T. C. Sangster, D. D. Meyerhofer, C. Stoeckl, J. M. Soures, P. A. Amendt, S. P. Hatchett, and R. E. Turner, "Use of Secondary Nuclear Particles for Studying the Areal Density of D_2-Filled Inertial Confinement Fusion Capsules," to be published in Physics of Plasmas.
11. T. C. Sangster, J. A. Delettrez, R. Epstein, V. Yu. Glebov, V. N. Goncharov, D. R. Harding, J. P. Knauer, R. L. Keck, J. D. Kilkenny, S. J. Loucks, L. D. Lund, R. L. McCrory, P. W. McKenty, F. J. Marshall, D. D. Meyerhofer, S. F. B. Morse, S. P. Regan, P. B. Radha, S. Roberts, W. Seka, S. Skupsky, V. A. Smalyuk, C. Sorce, J. M. Soures, C. Stoeckl, K. Thorp, J. A. Frenje, C. K. Li, R. D. Petrasso, F. H. Séguin, K. A. Fletcher, S. Padalino, C. Freeman, N. Izumi, J. A. Koch, R. A. Lerche, M. J. Moran, T. W. Phillips, and G. J. Schmid, Phys. Plasmas **10**, 1937 (2003).
12. Y. Lin, T. J. Kessler, and G. N. Lawrence, Opt. Lett. **20**, 764 (1995).
13. S. P. Regan, J. A. Marozas, J. H. Kelly, T. R. Boehly, W. R. Donaldson, P. A. Jaanimagi, R. L. Keck, T. J. Kessler, D. D. Meyerhofer, W. Seka, S. Skupsky, and V. A. Smalyuk, J. Opt. Soc. Am. B **17**, 1483 (2000).
14. T. R. Boehly, V. A. Smalyuk, D. D. Meyerhofer, J. P. Knauer, D. K. Bradley, R. S. Craxton, M. J. Guardalben, S. Skupsky, and T. J. Kessler, J. Appl. Phys. **85**, 3444 (1999).
15. C. Li and R. D. Petrasso, Phys. Plasmas **2**, 2460 (1995).
16. W. J. Karzas and R. Latter, Astrophys. J. Suppl. Ser. **6**, 167 (1961).
17. J. A. Koch, S. W. Haan, and R. C. Mancini, "Multispectral Imaging of Continuum Emission for Determination of Temperature and Density Profiles Inside Implosion Plasmas," to be published in the Journal of Quantitative Spectroscopy and Radiative Transfer.
18. V. A. Smalyuk, V. N. Goncharov, J. A. Delettrez, F. J. Marshall, D. D. Meyerhofer, S. P. Regan, and B. Yaakobi, Phys. Rev. Lett. **87**, 155002 (2001).
19. I. Golovkin, R. Mancini, S. Louis, Y. Ochi, K. Fujita, H. Nishimura, H. Shirga, N. Miyanaga, H. Azechi, R. Butzbach, I. Uschmann, E. Förster, J. Delettrez, J. Koch, R. W. Lee, and L. Klein, Phys. Rev. Lett. **88**, 045002 (2002).